Original Article

www.jmss.mui.ac.ir

Distribution of Intravascular and Extravascular Extracellular Volume Fractions by Total Area under Curve for Neovascularization Assessment by Dynamic Contrast-Enhanced Magnetic Resonance Imaging

Yi Sun

Department of Electrical Engineering, The City College of City University of New York, New York, NY, USA

Submission: 18-05-2013 Accepted: 25-04-2014

ABSTRACT

In this paper, we propose and investigate distribution of intravascular and extravascular extracellular volume fractions (DIEEF) as a noninvasive biomarker for neovascularization assessment by dynamic contrast-enhanced magnetic resonance imaging (DCE-MRI). A generalized two-compartment exchange model (G2CXM) that uniformly includes the Patlak model, Tofts model, extended Tofts model, and recent two-compartment exchange model as special instances is first presented. Based on the total area under curve of the G2CXM a method of DIEEF estimation without knowing the artery input function is proposed. The mean square error of DIEEF estimate in the presence of noise and with incomplete DCE-MRI data is analyzed. Simulation results demonstrate that DIEEF estimate is accurate when signal to noise ratio is only 5 dB in both cases of tracer infusion and bolus injection, and slightly favors the bolus injection. Tested on a model of atherosclerotic rabbits, the DIEEF of aorta plaques is positively correlated with the histological neovessel count with correlation coefficient of 0.940 and $P = 0.017$, and outperforms six semiquantitative parameters in the literature. DIEEF might be useful as a biomarker for noninvasive neovascularization assessment by DCE-MRI.

Key words: *Atherosclerosis, biomarker, dynamic contrast-enhanced magnetic resonance imaging, neovascularization, pharmacokinetics, tumor*

INTRODUCTION

Tumor growth needs vascular support and causes angiogenesis – an increase of neovessels and capillaries. Therefore an appropriate neovascularization assessment by estimation of physiological parameters in pharmacokinetics of dynamic contrast-enhanced magnetic resonance imaging (DCE-MRI) is a potentially useful and important noninvasive biomarker for tumor characterization, staging, and therapeutic efficacy monitoring.[1,2] In the literature, two kinds of parameters can be derived from DCE-MRI acquisitions: Quantitative and semiquantitative.[1] The former is model based, such as tracer transfer constant from plasma to tissue K^{trans} (volume fraction/min), rate constant of tracer refluxing from tissue to plasma K_{ep} (volume fraction/min), plasma volume fraction v_p, and extravascular extracellular volume fraction v_e.[1-5] The latter is model-free, such as maximum time intensity ratio (MTIR),[6] washout gradient, upslope gradient, maximum signal intensity, onset time,[7,8] and initial area under signal intensity curve (IAUC).[9,10] The most important quantitative and semiquantitative parameters are K^{trans} and IAUC, respectively, which were recommended as primary endpoints in phase 1/2a trials for anticancer therapeutics.[2] Quantitative parameters have the advantage of a clear relation to tissue physiology but are more difficult to extract from DCE-MRI acquisitions;[1] on the other hand, semiquantitative parameters are easier to calculate but have an unclear relation to tissue physiology.

The two most widely used pharmacokinetic models in DCE-MRI are the Tofts model (TM)[3,4]

$$C'(t) = K^{trans} C_a(t) - K_{ep} C(t) \quad (1)$$

and the extended Tofts model (ETM)[5]

$$C'(t) = v_p C_a'(t) + (K^{trans} + v_p K_{ep}) C_a(t) - K_{ep} C(t) \quad (2)$$

where tissue concentration $C(t)$ (mM) is measurable by DCE-MRI, $C_a(t)$ (mM) is plasma concentration of a feeding artery to tissue, and $K_{ep} = K^{trans}/v_e$. Another popularly used

Address for correspondence:
Prof. Yi Sun, Convent Avenue, 138th Street, New York, NY 10031, USA. E-mail: ysun@ccny.cuny.edu

pharmacokinetic model is the Patlak model.[11] If arterial input function (AIF) $C_a(t)$ can be obtained, these physiological parameters K^{trans}, v_p, and v_e can be estimated by data fitting on the basis of the models. However, to obtain AIF directly from DCE-MRI data is very difficult.[12-16] The common practice is to estimate an AIF from a main artery or vein near the tissue of interest or from a population of patients by average.[12-14] To avoid estimation of AIF the reference region (RR) method[15-25] can be applied. It assumes that the AIF for tissue of interest and tissue of reference is the same at any time instant. Then the common AIF $C_a(t)$ can be cancelled out from the pharmacokinetic models for both tissues. By fitting DCE-MRI data to the TM or ETM, the parameters K^{trans}, v_p, v_e of tissue of interest can be estimated as a function of the parameters of tissue of reference.[15-25]

Dynamic contrast-enhanced magnetic resonance imaging has been recently applied to characterization of atherosclerotic plaques on the basis of observation that their pathogenesis is associated with inflammation and neovascularization.[26,27] The studies in[28-31] applied a model that is built upon the observation that in a short period after tracer injection the tracer reflux from tissue to plasma is negligible. It is further assumed that the AIF $C_a(t)$ is an exponential function parameterized by amplitude and decay rate, which are estimated by fitting the function to signal of a main jugular vein close to artery of interest. Then parameters K^{trans} and v_p can be estimated from DCE-MRI data fitting to the simplified ETM model. In addition to study of quantitative parameters, a study on the semiquantitative parameter of IAUC for neovessel detection in atherosclerotic plaques was carried out.[32] It was found that the correlation between IAUC and histological neovessel count of atherosclerotic plaques for a rabbit model is positive.

In this paper, we propose and investigate the distribution of intravascular and extravascular extracellular volume fractions (DIEEF) as a noninvasive biomarker for neovascularization assessment. An estimation method of DIEEF based on the total area under curve (TAUC) of a generalized two-compartment exchange model (G2CXM)[33] is developed. The mean square error (MSE) of DIEEF is analyzed. DIEEF is then tested on a model of atherosclerotic rabbits and compared with six semiquantitative parameters. The method of DIEEF was partly presented in the previous study,[34] but this paper thoroughly presents the theory, simulation, and experimental results of DIEEF in a model of atherosclerotic rabbits.

THEORY AND METHODS

Generalized Two-compartment Exchange Model

Sourbron and Buckley[35] developed a two-compartment exchange model (2CXM) (Koh *et al*. recently presented the same model[36]) for stationary (time-invariant) linear tissues and proved that the TM and ETM are special instances of the 2CXM when $v_p \cong 0$ or $F_p \cong 0$ and when $v_p \cong 0$ or $F_p = \infty$, respectively, where F_p (1/min) is perfusion (blood flow). Tracer exchange through a capillary wall in the 2CXM is assumed to be bi-directionally symmetric. It is possible that a tissue includes an irreversible part as in the Patlak model[11] and therefore permeability is effectively asymmetric in two directions of capillary wall. To include tissues of asymmetric permeability in the model, the 2CXM was generalized to the G2CXM[33] defined by the system of equations

$$v_p C_p'(t) = F_p C_a(t) + P_e S C_e(t) - (F_p + P_p S) C_p(t) \quad (3)$$

$$v_e C_e'(t) = P_p S C_p(t) - P_e S C_e(t) \quad (4)$$

$$C(t) = v_p C_p(t) + v_e C_e(t) \quad (5)$$

$$C_a(t) = C_p(t) = C_e(t) = 0\,,\ t \le 0, \text{ or } t \ge T_w \quad (6)$$

As illustrated in Figure 1, $P_p > 0$ and $P_e > 0$ are permeability when tracer diffuses from plasma to extravascular extracellular space (EES) through the capillary wall and converse, respectively, S is surface area of capillary and $C_p(t)$ and $C_e(t)$ (mM) are tracer concentration in plasma and in EES, respectively. Eq. 6 means that tracer is injected at time zero and is completely washed out at time T_w.

The G2CXM allows asymmetric permeability $P_p \neq P_e$ and therefore uniformly includes the Patlak model ($P_e = 0$), TM, ETM, and 2CXM ($P_p = P_e = P$) as special instances. The method of DIEEF estimation developed on the basis of the G2CXM is applicable to the Patlak, TM, ETM, and 2CXM as well as tissues of asymmetric permeability. All parameters in the model are normalized to tissue volume that is assumed to be unit throughout and therefore $v_p + v_e \le 1$.

Like the 2CXM the G2CXM accommodates to a broad range of pharmacokinetic parameter values and therefore is suitable for characterization of a variety of tissues. In particular, v_p, v_e and F_p in the G2CXM can take various values and hence

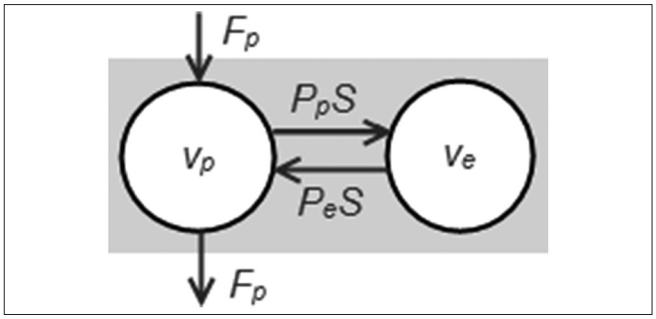

Figure 1: The generalized two-compartment exchange model for a tissue of interest (the shaded region). F is blood flux, v_p and v_e are intravascular volume fraction and extravascular extracellular volume fraction, respectively, S is surface area of capillary, P_p is permeability from plasma to extravascular extracellular space (EES), and P_e is permeability from EES to plasma. P_p and P_e can be different

tumors that are heterogeneous in neovascularization and perfusion at different stages[1,37] can be characterized. In addition to tumors, it has been evidenced that certain types of atherosclerotic plaques are rich in neovasculature[28-31] that is one of the key pathological factors in characterizing atherosclerotic plaques and prediction of precipitate acute clinic events.[26,27] Hence, the G2CXM is also suitable for neovascularization assessment of atherosclerotic plaques.

Definition of Distribution of Intravascular and Extravascular Extracellular Volume Fractions

Consider all M tissues in the region of view, of which DCE-MRI signals can be acquired in a scan. Concentration of the i^{th} tissue $C_{\text{i}}(t)$ satisfies the G2CXM, $i = 1, 2,\ldots, M$.

$$v_{\text{p,i}}C'_{\text{p,i}}(t) = F_{\text{p,i}}C_{\text{a,i}}(t) + P_{\text{e,i}}S_{\text{i}}C_{\text{e,i}}(t) - (F_{\text{p,i}} + P_{\text{p,i}}S_{\text{i}})C_{\text{p,i}}(t) \quad (7)$$

$$v_{\text{e,i}}C'_{\text{e,i}}(t) = P_{\text{p,i}}S_{\text{i}}C_{\text{p,i}}(t) - P_{\text{e,i}}S_{\text{i}}C_{\text{e,i}}(t) \quad (8)$$

$$C_{\text{i}}(t) = v_{\text{p,i}}C_{\text{p,i}}(t) + v_{\text{e,i}}C_{\text{e,i}}(t) \quad (9)$$

The G2CXM can be applied to tissues of different size and shape. However, in general the G2CXM shall be applied to a voxel (or pixel in 2-D data) tissue, a segment of arterial wall, or a tumor consisting of a number of voxels, which is a small part in the region of view. A wide-sense DIEEF for the M tissues is defined as

$$p_{\text{i}} = \frac{v_{\text{p,i}} + (P_{\text{p,i}}/P_{\text{e,i}})v_{\text{e,i}}}{\sum_{j=1}^{M}(v_{\text{p,j}} + (P_{\text{p,j}}/P_{\text{e,j}})v_{\text{e,j}})}, i = 1, 2,\ldots, M \quad (10)$$

The wide-sense DIEEF defined in Eq. 10 depends only on physiological parameters of tissues: Intravascular and extravascular extracellular volume fractions (IEEF) and permeabilities of capillary walls of tissues in the region of view. Strictly speaking, the wide-sense DIEEF does not have physiological meaning of DIEEF defined by

$$p_{\text{i}} = \frac{v_{\text{p,i}} + v_{\text{e,i}}}{\sum_{j=1}^{M}(v_{\text{p,j}} + v_{\text{e,j}})}, i = 1, 2,\ldots, M \quad (11)$$

that is a special instance when tissues have symmetric permeability $P_{\text{p,i}} = P_{\text{e,i}}$ in two directions of capillary wall; in this case, the G2CXM is degenerated to the 2CXM. However, wide-sense DIEEF captures effect of asymmetric permeability of capillary wall in the total tissue concentration as if a tissue had the extravascular extracellular volume fraction $(P_{\text{p,i}}/P_{\text{e,i}})v_{\text{e,i}}$. The larger the ratio $P_{\text{p,i}}/P_{\text{e,i}}$ is, the larger the effective EES is. Due to this, the wide-sense DIEEF may be useful in characterizing tumors that have poorly formed and fragile vessels with high and heterogeneous permeability.[1] On the other hand, when applied to tissues that are prior known to have a symmetric capillary wall, an estimated DIEEF shall be interpreted as Eq. 11. Henceforth, the wide-sense DIEEF will be simply called DIEEF. Summation of p_{i} over all tissues equals one as a probability distribution does.

If all tissues have very low vasculature $v_{\text{p, i}} \cong 0$, DIEEF degenerates to distribution of extravascular extracellular volume fractions (DEEF)

$$p_{\text{i}} = \frac{(p_{\text{p,i}}/p_{\text{e,i}})v_{\text{e,i}}}{\sum_{j=1}^{M}(p_{\text{p,j}}/p_{\text{e,j}})v_{\text{e,j}}}, i = 1, 2,\ldots, M \quad (12)$$

and if moreover all tissues have symmetric permeability $P_{\text{p, i}} = P_{\text{e, i}}$, then

$$p_{\text{i}} = \frac{v_{\text{e,i}}}{\sum_{j=1}^{M}v_{\text{e,j}}}, i = 1, 2,\ldots, M \quad (13)$$

in this case, the G2CXM is degenerated to the TM in Eq. 1 with $K^{\text{trans}} = F_{\text{p}}PS/(F_p + PS)$.[35]

Distribution of intravascular and extravascular extracellular volume fractions p_i of a tissue measures IEEF $v_{\text{p,i}} + (p_{\text{p,i}}/p_{\text{e,i}})v_{\text{e,i}}$ relative to all other tissues in the region of view. Like K^{trans}, IEEF is a composite of physiological parameters and hence is DIEEF. However, unlike a quantitative parameter, DIEEF does not measure the absolute value of IEEF but the value relative to others.

We hypothesize that DIEEF p_i of a tissue is positively correlated to its neovessel count in histology and therefore indicates degree of neovascularization and inflammation. A reason is that a high intravascular volume fraction $v_{\text{p, i}}$ indicates a large count of neovessels and capillaries and therefore indicates a high degree of neovascularization. However, how $(p_{\text{p,i}}/p_{\text{e,i}})v_{\text{e,i}}$ is correlated to neovascularization is worthy to be studied for various types of tissues. The hypothesis is tested on a model of atherosclerotic rabbits in this study.

Method of Estimation

The TAUC of the i^{th} tissue is defined as $\int_0^{T_{\text{w}}} C_{\text{i}}(t)dt$. Due to the boundary condition in Eq. 6, taking integral over Eqs. 7, and (8), respectively, we can obtain that tissue TAUC and plasma TAUC are related by

$$\int_0^{T_{\text{w}}} C_{\text{i}}(t)dt = \left(v_{\text{p,i}} + (p_{\text{p,i}}/p_{\text{e,i}})v_{\text{e,i}}\right)\int_0^{T_{\text{w}}} C_{\text{a,i}}(t)dt \quad (14)$$

If plasma TAUCs are the same for all tissues, that is,

$$\int_0^{T_{\text{w}}} C_{\text{a,i}}(t)dt = \int_0^{T_{\text{w}}} C_{\text{a}}(t)dt \text{ for all } i, \quad (15)$$

then DIEEF can be determined by tissue TAUCs as

$$p_{\mathrm{i}} = \frac{\int_0^{T_{\mathrm{w}}} C_{\mathrm{i}}(t)dt}{\sum_{j=1}^{M}\int_0^{T_{\mathrm{w}}} C_{\mathrm{j}}(t)dt}, i = 1, 2,\ldots, M. \quad (16)$$

The condition in Eq. 15 can be approximately satisfied if all tissues are close to each other or if feeding arteries of all tissues are braches of a main artery. This condition means that all tissues experience the same amount of average plasma concentration, but not necessarily the same AIF at each time instant. In comparison, the RR method assumes that AIF's of tissue and reference are equal at each time instant t.

In practice, DCE-MRI signal is usually acquired in a period [0, T] of time before tracer is completely washed out, that is, $T < T_{\mathrm{w}}$. Let the time average of acquired signal $C_{\mathrm{i}}(t)$ be

$$< C_{\mathrm{i}} > \equiv \frac{1}{T}\int_0^{T} C_{\mathrm{i}}(t)dt \quad (17)$$

Then DIEEF is estimated by

$$\bar{p}_{\mathrm{i}} = \frac{< C_{\mathrm{i}} >}{\sum_{j=1}^{M} < C_{\mathrm{j}} >}, i = 1, 2,\ldots, M \quad (18)$$

An incomplete data acquisition yields a residual error that will be analyzed in the next subsection. Removal of the constant 1/T in Eq. 17 does not change the estimate; however, for the purpose of analysis and understanding of estimation error we use the time average instead of integral in estimate.

In practice, $C_{\mathrm{i}}(t)$ in [0, T] is sampled at discrete time Δk for $k = 0, 1,\ldots, N-1$ where Δ (s) is temporal resolution. The differential equations in Eqs. 7-9 become difference equations

$$C_{\mathrm{p,i}}(k+1) = \frac{\Delta F_{\mathrm{p,i}}}{v_{\mathrm{p,i}}} C_{\mathrm{a,i}}(k) + \frac{\Delta P_{\mathrm{e,i}} S_{\mathrm{i}}}{v_{\mathrm{p,i}}} C_{\mathrm{e,i}}(k) + \left(1 - \frac{\Delta(F_{\mathrm{p,i}} + P_{\mathrm{p,i}} S_{\mathrm{i}})}{v_{\mathrm{p,i}}}\right) C_{\mathrm{p,i}}(k) \quad (19)$$

$$C_{\mathrm{e,i}}(k+1) = \frac{\Delta P_{\mathrm{p,i}} S_{\mathrm{i}}}{v_{\mathrm{e,i}}} C_{\mathrm{p,i}}(k) + \left(1 - \frac{\Delta P_{\mathrm{e,i}} S_{\mathrm{i}}}{v_{\mathrm{e,i}}}\right) C_{\mathrm{e,i}}(k) \quad (20)$$

$$C_{\mathrm{i}}(k) = v_{\mathrm{p,i}} C_{\mathrm{p,i}}(k) + v_{\mathrm{e,i}} C_{\mathrm{e,i}}(k) \quad (21)$$

where $C_{\mathrm{i}}(k+1)$ denotes $C_{\mathrm{i}}(\Delta(k+1))$ and hence accordingly do other concentrations. The time average in Eq. 17 becomes $< C_{\mathrm{i}} >= \frac{1}{N}\sum_{k=0}^{N-1} C_{\mathrm{i}}(k)$. In practice, only noisy tissue concentration

$$y_{\mathrm{i}}(k) = C_{\mathrm{i}}(k) + n_{\mathrm{i}}(k) \quad (22)$$

can be acquired where $n_{\mathrm{i}}(k)$ represents noise. The time average of noisy $y_{\mathrm{i}}(k)$ is actually used in the estimation of DIEEF

$$\hat{p}_{\mathrm{i}} = \frac{< y_{\mathrm{i}} >}{\sum_{j=1}^{M} < y_{\mathrm{j}} >}, i = 1, 2,\ldots, M \quad (23)$$

The time average of noisy tissue concentration is

$$< y_{\mathrm{i}} > = < C_{\mathrm{i}} > + < n_{\mathrm{i}} > \quad (24)$$

where $< n_{\mathrm{i}} >$ denotes time average of $n_{\mathrm{i}}(k)$

Estimation Error

To better understand how to obtain a reliable estimate of DIEEF, analysis of estimation error is necessary. The estimation error between $\hat{p}_{\mathrm{i}}$ and p_{i} is incurred by two factors. First, when a DCE-MRI signal used in DIEEF estimation is incomplete, that is, $T < T_{\mathrm{w}}$, there is a residual error between $\bar{p}_{\mathrm{i}}$ and p_{i}. Second, in the presence of noise there is an error between $\hat{p}_{\mathrm{i}}$ and $\bar{p}_{\mathrm{i}}$. Since the error caused by noise is random, we can use MSE to measure error of DIEEF estimate for the i^{th} tissue as

$$\mathrm{MSE}_{\mathrm{i}} = E[(\hat{p}_{\mathrm{i}} - p_{\mathrm{i}})^2] \quad (25)$$

where E denotes probabilistic mean. The MSE indicates an error of DIEEF estimate different from its true value. The MSE can be decomposed into

$$\mathrm{MSE}_{\mathrm{i}} = E[(\hat{p}_{\mathrm{i}} - \bar{p}_{\mathrm{i}})^2] + 2(\bar{p}_{\mathrm{i}} - p_{\mathrm{i}})E(\hat{p}_{\mathrm{i}} - \bar{p}_{\mathrm{i}}) + (\bar{p}_{\mathrm{i}} - p_{\mathrm{i}})^2 \quad (26)$$

The first term is the MSE between $\hat{p}_{\mathrm{i}}$ and $\bar{p}_{\mathrm{i}}$ due to noise and the last term is called square residual error (SRE) that is nonzero when a DCE-MRI signal is incomplete. By MSE_i Eq. 25 the root MSE

$$\mathrm{RMSE}_{\mathrm{i}} = \sqrt{\mathrm{MSE}_{\mathrm{i}}}\,/\,p_{\mathrm{i}} \quad (27)$$

and the error over all tissues

$$\mathrm{RMSE} = \sqrt{\sum_{i=1}^{M} \mathrm{MSE}_{\mathrm{i}} \Big/ \sum_{i=1}^{M} p_{\mathrm{i}}^2} \quad (28)$$

can also be calculated.

As will be seen, estimation errors are determined by signal to noise ratio (SNR) of an acquired DCE-MRI signal. To this end, we first discuss noise statistics and define SNR of related signals. It is known that the noise in magnitude of MRI data has a Rician distribution. When signal to noise amplitude ratio is >2, a Rician distribution can be well

approximated by a Gaussian distribution.[38] Since tracer significantly increases signal amplitude, it is rational to assume that noise $n_i(k)$ is Gaussian distributed with mean zero and variance σ^2; and due to whiteness of noise process,[38] noise samples $n_i(k)$ across tissue i and time k are mutually independent.

Signal to noise ratio measures quality of an acquired DCE-MRI signal. Although DIEEF estimation does not need a measurement of AIF, the SNR of AIF can be used as an index of signal quality when errors of DIEEFs are evaluated. Hence, we consider the scenario that in a scan of noisy tissue concentration $y_i(k)$, a noisy AIF was also measured. where noise $m_i(k)$ has the same statistics of $n_i(k)$ due to the same scanner. The signal power is $< C_{a,i}^2 >$ that is time average of $C_{a,i}^2(k)$ and the noise power is $E(< m_i^2 >) = \sigma^2$. By adapting the standard definition,[39] SNR of AIF $y_{a,i}(k)$ is

$$\begin{aligned} \mathrm{SNR}_{a,i} &= \frac{< C_{a,i}^2 >}{E(< m_i^2 >)} \\ &= 10\log_{10}\left(\frac{< C_{a,i}^2 >}{\sigma^2}\right)(\mathrm{dB}) \end{aligned} \tag{29}$$

Similarly, SNR of noisy concentration of tissues $y_i(k)$ is

$$\begin{aligned} \mathrm{SNR}_i &= \frac{< C_i^2 >}{E(< n_i^2 >)} \\ &= 10\log_{10}\left(\frac{< C_i^2 >}{\sigma^2}\right)(\mathrm{dB}) \end{aligned} \tag{30}$$

As a convention, unit of decibel (dB) is used in SNR so that a wide range of SNR can be considered.

Note that $\mathrm{SNR}_{a,i}$ and SNR_i are for raw DCE-MRI data without processing. After the processing of time averaging, $< y_i >$ has signal power $< C_i >^2$ and noise power $E(< n_i >^2) = \sigma^2/N$ where the equality is due to independence of noise samples. Then SNR of $< y_i >$ is

$$\begin{aligned} \mathrm{SNR}_i^{\mathrm{ave}} &= \frac{< C_i >^2}{E(< n_i >^2)} = \frac{N < C_i >^2}{\sigma^2} \\ &= 10\log_{10}\left(\frac{N < C_i >^2}{\sigma^2}\right)(\mathrm{dB}) \end{aligned} \tag{31}$$

It is clear that $\mathrm{SNR}_{a,i}$ does not depend on the tissue parameters but SNR_i and $\mathrm{SNR}_i^{\mathrm{ave}}$ do. Given AIF $C_{a,i}(k)$, $\mathrm{SNR}_{a,i}$ is determined; and given AIF $C_{a,i}(k)$ and tissue parameters, SNR_i and $\mathrm{SNR}_i^{\mathrm{ave}}$ are determined via the G2CXM.

An AIF $C_{a,i}(t)$ is usually proportional to the concentration of tracer injection. Since the G2CXM is linear, tissue concentration $C_i(t)$ is also proportional to concentration of tracer injection. Consequently, if the concentration of tracer injection is increased by a factor of $\alpha > 1$, then all three SNRs are increased by $20\log_{10}\alpha$ dB. For example, doubling the concentration of tracer injection increases all SNRs by 6 dB.

We can show that $\mathrm{SNR}_i \le \mathrm{SNR}_i^{\mathrm{ave}} \le N\mathrm{SNR}_i$ where the second equality holds if and only if $C_i(k) = C_i$ is a constant for all k. The first inequality is obtained by $C_i(k) \ge 0$ and the second inequality is due to the convexity of a square function. This implies that average of tissue concentration always increases SNR and the maximum increase is $10\log_{10}(N)$ dB.

Based on the statistics of noise and definition of SNR, we can obtain that

$$\mathrm{MSE}_i = E\left[\left(\frac{u + \sqrt{\mathrm{SNR}_i^{\mathrm{ave}}}}{u + (M-1)z + \sum_{j=1}^{M}\sqrt{\mathrm{SNR}_j^{\mathrm{ave}}}} - p_i\right)^2\right] \tag{32}$$

where u and z are independent standard Gaussian random variables with zero mean and unit variance. MSE_i, root mean square error (RMSE_i) and RMSE can be numerically evaluated by Eqs. 32, 27, and 28. Eq. 32 shows how AIF, physiological parameters, number of samples N or acquisition time T, and noise power σ^2 affect MSE_i. In general, as plasma TAUC, $v_{p,i}$, $v_{e,i}$, $p_{p,i}$, and N (or T) increase or $p_{e,i}$ and σ^2 decrease, $\mathrm{SNR}_i^{\mathrm{ave}}$ increases and then MSE_i decreases. However, these changes only reduce the effect of noise. As $\mathrm{SNR}_i^{\mathrm{ave}}$ increases, MSE_i eventually approaches its SRE $(\bar{p}_i - p_i)^2$, and RMSE_i and RMSE converge to the root SRE $\mathrm{RSRE}_i = |\bar{p}_i - p_i|/p_i$ and overall SRE by the root square residual error (RSRE)

$$\mathrm{RSRE} = \sqrt{\sum_{i=1}^{M}(\bar{p}_i - p_i)^2 \Big/ \sum_{i=1}^{M} p_i^2}$$

for all tissues, respectively. SRE is > 0 when an acquired DCE-MRI signal is incomplete. It follows from Eqs. 7-9 that

$$< C_i(t) >= \left(v_{p,i} + (P_{p,i}/P_{e,i})v_{e,i}\right) < C_{a,i}(t) > - w_i \tag{33}$$

where

$$w_i = \left(v_{p,i} + (P_{p,i}/P_{e,i})v_{e,i} + \frac{F_{p,i}v_{e,i}}{P_{e,i}S_i}\right)\frac{C_i(T)}{TF_{p,i}} - \frac{v_{p,i}v_{e,i}C_{p,i}(T)}{P_{e,i}S_iT} \tag{34}$$

Denote $A_i = \left(v_{p,i} + (p_{p,i}/p_{e,i})v_{e,i}\right) < C_{a,i} >$ Then SRE can be calculated by

$$(\bar{p}_i - p_i)^2 = \left(\frac{A_i\sum_{j=1}^{M} w_j - w_i\sum_{j=1}^{M} A_j}{\sum_{k=1}^{M} A_k \sum_{j=1}^{M}(A_j - w_j)}\right)^2 \tag{35}$$

Post the transient time, tracer concentrations in all compartments decay to wash out through the kidney and so $C_i(T)$ and $C_{p,i}(T)$ monotonically decreases as T increases. Eq. 34 indicates that the residual error decreases as T increases. If an acquired signal of tissue concentration $C_i(t)$ is complete, that is, $T = T_w$, SRE is equal to zero due to $C_i(T_w) = C_{p,i}(T_w) = 0$. Note that, the TAUC used in DIEEF estimation is different from the conventional IAUC.[9,10] First, a physiological meaning of IAUC is unclear. Second, the conventional IAUC emphasizes use of the initial signal of tissue concentration, but the TAUC requires use of all acquired signal and the acquisition time T is as long as possible. Using the IAUC in estimation of DIEEF would cause a large estimation error. This is verified by the simulation in the next section.

Both tracer infusion and bolus injection can be used in estimation of DIEEF. However, bolus injection can make washout time slightly shorter and therefore is slightly better regarding reducing the effect of incompleteness of data.

Experiments

Simulation

Simulations are carried out to demonstrate effect of physiological parameters $v_{p,i}$, $v_{e,i}$, $P_{p,i}S$, $P_{e,i}S$, $F_{p,i}$, acquisition time T, and SNR on estimation error. To simplify the simulations and without loss of generality, all tissues are considered to have the same AIF; therefore, AIF SNR_a in Eq. 29 is equal for all tissues. Given an AIF, tissue concentrations are iteratively obtained by Eqs. 19-21 with $C_i(0) = 0$ and $\Delta = 2$ s. In each trial $y_i(k)$ is generated by adding independent Gaussian noise samples $n_i(k)$ to $C_i(k)$ and then DIEEF is estimated by Eq. 23, resulting in a sample square error $(\hat{p}_i - p_i)^2$. At each SNR_a the sample MSE_i is obtained by averaging $(\hat{p}_i - p_i)^2$ over one thousand trials; that is, the simulation is run one thousand times with randomly generated noise samples. The theoretical MSE_i is also calculated by Eq. 32 and is compared with the sample MSE_i. $RMSE_i$ and RMSE in both simulation and theory are then obtained by Eqs. 27 and 28.

Two AIFs are considered, simulating an infusion and a bolus injection, respectively. In both cases, 36 tissues with all combinations of $(v_p, v_e) \in \{(0.15, 0.2), (0.15, 0.5), (0.15, 0.85), (0.4, 0.2), (0.5, 0.5), (0.7, 0.25)\}$, $(P_pS, P_eS) \in \{(0.65, 0.65), (0.85, 0.65), (0.85, 0.85)\}$ (/min,/min), and $F_p \in \{0.75, 1.8\}$ (/min) are considered. These values cover most range of the parameters. The results of five representative tissues (out of 36) are illustrated in figures with the parameters given in Table 1 where their IEEFs are purposely listed in the descent order.

Infusion

In the simulation of an infusion, the AIF exponentially increases immediately after tracer injection, holds a constant, and then exponentially decays to washout

$$C_a(t) = \begin{cases} (a/b)t\exp(1-t/b), & 0 \le t \le b, \\ a, & b < t \le c, \\ a\exp((c-t)/d), & t > c, \end{cases} \quad (36)$$

where $a = 1.2$ mM, $b = 1$ min, $c = 6$ min, $d = 40$ min. Figure 2 shows the AIF $C_a(t)$ for $T = 16$ min, concentrations $C_i(k)$ and their noisy observations $y_i(k)$ of the five representative tissues. To respond to the AIF, tissue concentrations quickly rise in the transient period of about [0, 5] min, reach a plateau and then decay slowly to wash out. In the total period [0, 16] min of acquisition, AIF power is equal to $< C_a^2 > \cong 1.210$ and noise power is purposely set to $\sigma^2 \cong 1.210 \times 10^{-2}$ so that AIF SNR_a in Eq. 29 is 20 dB. Correspondingly, the five representative tissues have $SNR_i = 20.84, 20.00, 19.47, 16.06, 10.67$ dB for $i = 1,\ldots, 5$, which decrease as IEEF decreases, accordingly to Eq. 14.

Figure 3 illustrates estimation errors RMSE and $RMSE_i$ versus AIF SNR_a when DIEEF is estimated using $y_i(k)$ for [0, 16] min. $RMSE_i$ varies with tissue since SNR_i of a tissue concentration varies with IEEF. In the low SNR_a regime, RMSE and $RMSE_i$ are dominated by noise, particularly for those tissues with a small IEEF. However, even when AIF SNR_a is only 5 dB, DIEEF overall is reliably estimated with RMSE ≅ 5% and therefore is robust to noise. As SNR_a increases, RMSE and $RMSE_i$ monotonically decrease and

Table 1: Parameters of five representative tissues

i	$v_{p,i}$	$v_{e,i}$	$P_{p,i}S$	$P_{e,i}S$	$F_{p,i}$	IEEF
1	0.50	0.50	0.85	0.65	1.80	1.15
2	0.70	0.25	0.85	0.65	1.80	1.03
3	0.15	0.85	0.85	0.85	1.80	1.00
4	0.40	0.20	0.85	0.65	0.75	0.66
5	0.15	0.20	0.65	0.65	0.75	0.35

IEEF – Intravascular and extravascular extracellular volume fraction

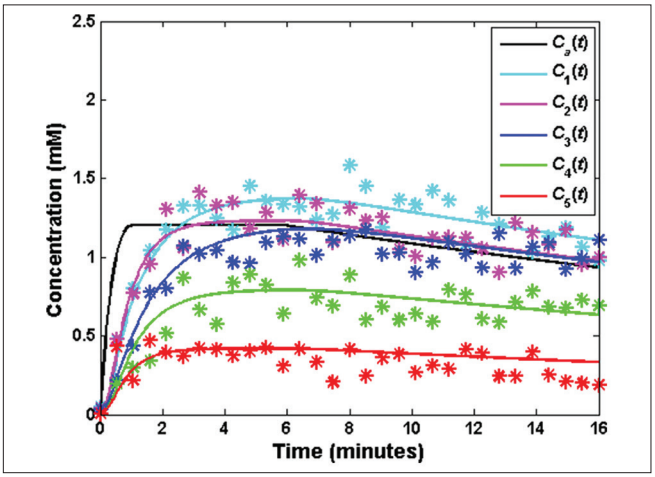

Figure 2: Case of infusion: Arterial input function $C_a(t)$ and $C_i(t)$ for $i = 1, 2, 3, 4, 5$ as well as their noisy observations $y_i(k)$ of the five representative tissues in Table 1. Stars are part of $y_i(k)$ samples

eventually approach, respectively, RSRE and $RSRE_i$ (4% and lower) when SNR = ∞, which is due only to incompleteness of data used in the DIEEF estimation. Figure 4 illustrates how estimation errors RMSE and $RMSE_i$ (and RSRE and $RSRE_i$ as well) vary with acquisition time T. When acquisition time is within the transient period prior to 5 min, all RMSE and $RMSE_i$ are large, particularly for those having a small IEEF. This indicates that use of IAUC to replace TAUC in the DIEEF estimation would yield large errors. In the low SNR_a regime, RMSE and $RMSE_i$ are dominated by noise and so are monotonically decreasing; and in the high SNR_a regime, errors are convex down in most cases. However, post the transient time, as T increases, errors in all SNR_a monotonically decrease to a small value about 5%. Hence, performance of DIEEF is low and improves quickly during the transient time and is eventually high and stable post the transient time. Figures 3 and 4 also demonstrate that the theoretical formula in Eq. 32 predicts estimation errors in the simulation.

Bolus injection

In the simulation of a bolus injection, the following exponential AIF ordinary in the literature[25] is used

$$C_a(t) = at^b \exp(-t/c) + d(1-\exp(-t/g))\exp(-t/h) \qquad (37)$$

where a = 18.0 mM, b = 1, c = 0.25 min, d = 1.1 mM, g = 0.2 min, h = 25 min with Δ = 2 s.

As illustrated in Figure 5, the AIF $C_a(t)$ with T = 16 min presents a narrow and high peak and then decays slowly to wash out. To respond to the AIF, tissue concentrations $C_i(t)$ increase rapidly in the short transient time of about [0, 3] min and then present a plateau decaying slowly. In the entire period of [0, 16] min, AIF power is equal to $< C_a^2 > \cong 0.859$ and noise power is purposely set to $\sigma^2 \cong 8.59 \times 10^{-3}$ so that AIF SNR_a is 20 dB. The five representative tissues have correspondingly SNR_i = 20.44, 19.67, 19.03, 15.67, 10.35 dB for i = 1,…, 5.

As demonstrated in Figures 6 and 7, all results are similar to those in the case of infusion. However, the bolus injection takes slightly shorter time to washout and with given T the data in the bolus injection are closer to completeness; and therefore all errors are smaller than those in the case of infusion. This suggests that DIEEF estimation favors a bolus injection.

Test on a model of atherosclerotic rabbits

The animal data used in this study is in,[32] including the MRI data and histological neovessel counts of aorta plaques in five rabbits. The reader is referred to[32] for technical details in animal treatment and data acquisition. The MRI data were acquired using a bolus injection. For each of five rabbits, a sequence of 150 images with a size of 256 × 256 were acquired at a temporal resolution of 4.8 s and a spatial resolution of 470 μm × 470 μm. Figure 8 shows MRI images of a representative rabbit acquired at time 0.4 and 3.6 min, respectively. Since tracer was injected after acquisition of the 5th image at time 0.4 min, the left image does not show tracer and the right does.

A DIEEF image for each rabbit shall be produced, which references neovascularization of aorta – the tissue of interest – and the DIEEF value of aorta shall be comparable with those of other rabbits in neovascularization assessment. To this end, the following steps were taken.

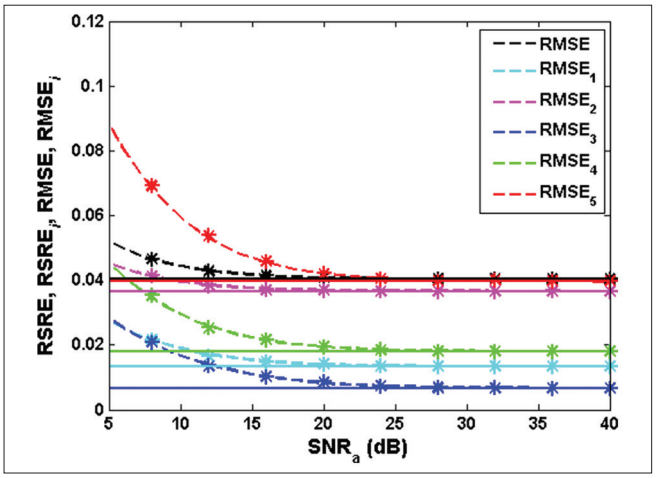

Figure 3: Distribution of intravascular and extravascular extracellular volume fractions (DIEEF) is estimated by using $y_i(k)$ for [0, 16] min in Figure 2. Dashed lines are root mean square error (RMSE) (for all 36 tissues) and $RMSE_i$ of the five representative tissues, respectively, calculated by Eq. 32, versus arterial input function signal to noise ratio (SNR_a). Stars are simulation results. Solid lines are root square residual error (RSRE) and $RSRE_i$ corresponding to the RMSE and $RMSE_i$ at SNR_a = ∞ dB, respectively

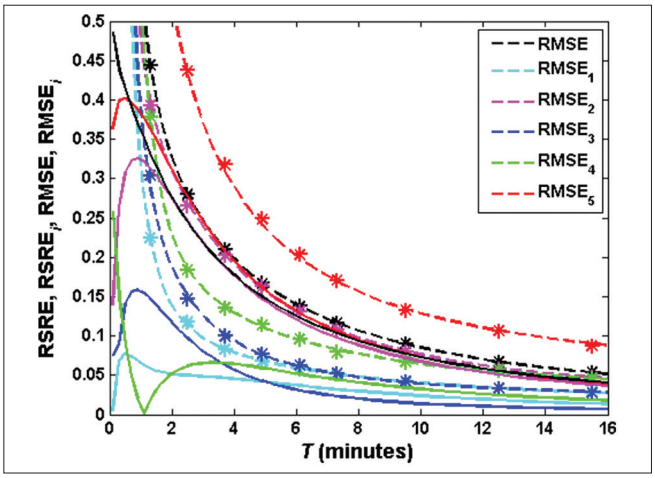

Figure 4: RSRE, $RSRE_i$, RMSE and $RMSE_i$ are versus acquisition time T for the signal in Figure 2. Dashed lines are RMSE and $RMSE_i$ calculated by Eq. 32 with arterial input function signal to noise ratio (SNR_a) = 5 dB, and stars are the corresponding simulation results. Solid lines are RSRE and $RSRE_i$ corresponding to SNR = ∞ dB. For 5 ≤ SNR_a < ∞ dB, RMSE and $RMSE_i$ are between the dashed and solid lines. For $T \geq 6$ min, RMSE and $RMSE_i$ are already small and monotonically decrease

- Step 1: Produce DCE-MRI image sequence. Tracer emerged in the tissue around 0.8 min. The first ten MRI images that apparently show no effect of tracer were averaged to form a base image that has 10 dB higher SNR than the original images and hence is reliable. A sequence of DCE-MRI images was obtained by subtracting the base image from each of the 150 images. A DCE-MRI image (not presented) shows the trace concentrations $C_i(t)$ in each pixel i at a time instant t.
- Step 2: Select region of view. Data in region of view will be used in DIEEF estimation. In general, region of view shall be relatively large and can provide a stable and reasonable reference to the tissue of interest (i.e. the aorta). In a homogeneous population such as rabbits, region of view can include all tissues except the kidney. In a heterogeneous population, region of view can be smaller and enclose tissue of interest, or a fixed region of muscle enclosing or nearby tissue of interest. The reasons here to exclude the kidney from region of view are (a) the G2CXM is not applicable to the kidney that allows tracer washout from EES and therefore is modeled differently;[40] (b) since a large amount of tracer is collected by the kidney, if included in the region of view, a minor variation of kidney data would significantly bias DIEEF estimate. Hence, in this study the region of view is chosen to include all tissues in the scan except the kidney. Figure 9 demonstrates the curves of averages over the region of view for the five rabbits.
- Step 3: Produce DIEEF image. The DCE-MRI images used in DIEEF estimation are the 141 images from image 10 (0.8 min) through 150 (12 min). The effective acquisition time from the emergence of tracer to the end of acquisition is $T = 11.2$ min. DIEEF value of each pixel was estimated by Eq. 23, which produces the DIEEF image for a rabbit. Different from a DCE-MRI image $C_i(t)$, a DIEEF image shows the DIEEF p_i at each pixel i. Figure 10 illustrates the DIEEF image of the representative rabbit. A pixel intensity in a DIEEF image is the IEEF relative to others and therefore indicates

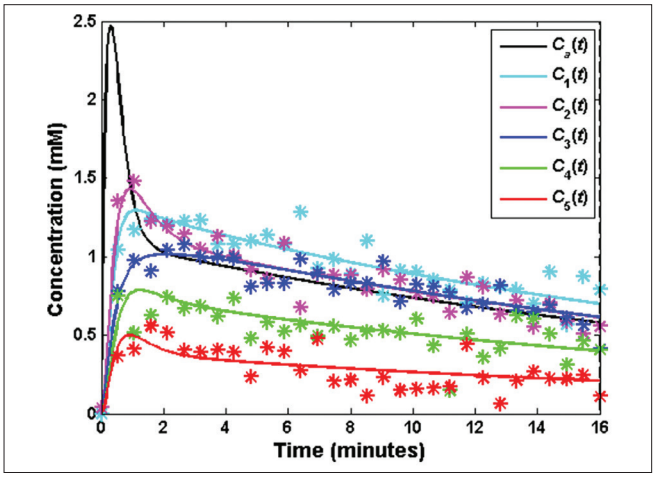

Figure 5: Case of bolus injection: The meanings of the curves are the same as those in Figure 2

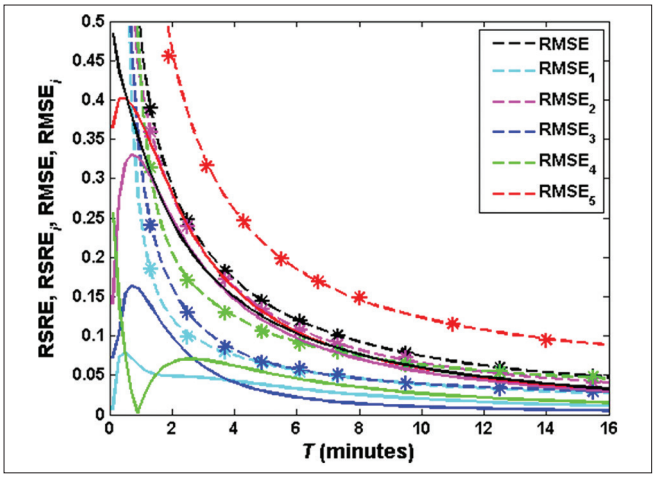

Figure 7: RSRE, RSRE$_i$, RMSE and RMSE$_i$ are versus acquisition time T for the signal in Figure 5. The meanings of the curves are the same as those in Figure 4

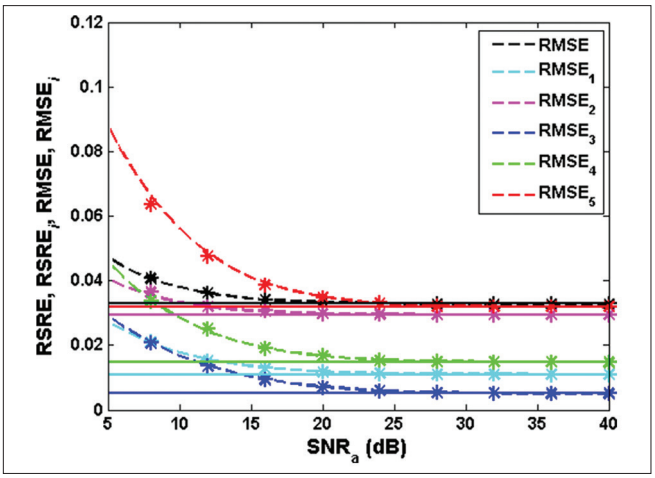

Figure 6: DIEEF is estimated by using $y_i(k)$ in Figure 5 during [0, 16] min. The meanings of the curves are the same as those in Figure 3

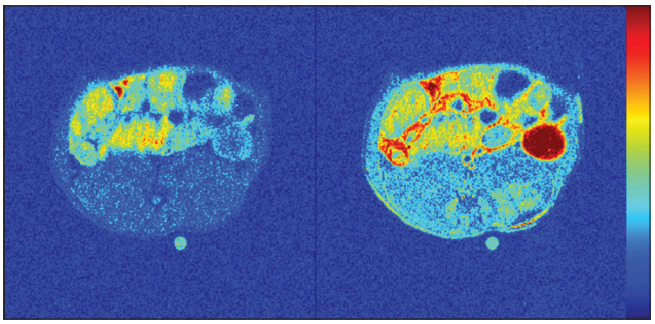

Figure 8: The magnetic resonance images of a representative rabbit acquired at time 0.4 (left) and 3.6 (right) min, respectively. The palette from top to bottom shows intensity descent. The left image does not show effect of tracer and the right does. The bright region in the right image is the kidney showing collection of a large amount of tracer

neovascularization relative to others in the sense of added variation by extravascular extracellular volume fraction.

- Step 4: Calculate DIEEF value of tissue of interest. DIEEF value of atherosclerotic plaque of a rabbit was obtained by averaging the pixels of DIEEF image over the aorta wall shown at the bottom-left corner in Figure 10.

To examine efficacy of DIEEF in neovascularization assessment, the correlation coefficient between DIEEF and histological neovessel count of aorta plaques in the five rabbits was calculated using all data in 12 min, which is $r = 0.940$ with $P = 0.017$, showing a high positive correlation. Figure 11 illustrates DIEEFs of aorta plaques versus histological neovessel counts, linear regression, and 95% confidence interval.

Effect of acquisition time

To examine how acquisition time affects performance of DIEEF, Table 2 presents the correlation coefficients between DIEEF of aorta plaques and neovessel counts and P values for 11 acquisition times where the effective acquisition time T' starts at 0.8 min when tracer emerges. It illustrates that during the transient time at the total time of about 3 min, the correlation coefficient is small and then increases quickly, and is relatively high and stable post the transient time. This confirms the simulation result that estimation error is large and decreases quickly during the transient time and reaches a small value post the transient time.

Meanwhile, it is found that as acquisition time increases, the estimate of plaque DIEEF for all five rabbits increases slowly with certain variations. It is interesting to test performance of DIEEF in the simulation case that a number of medical centers estimate plaque DIEEF by randomly selecting one of 10 acquisition times of $T = 2.96$, 4.00, 4.96, 6.00, 6.96, 8.00, 8.96, 10.00, 10.96, 12.00, all longer than the transient time, and a center uses the same selected acquisition time for all five rabbits. It is obtained that using all the 50 plaque DIEEF values (10 for each rabbit), the correlation coefficient between plaque DIEEF and neovessel count is 0.924, which is high and slightly lower than 0.940, with $P = 1.02 \times 10^{-21}$. This implies that DIEEF estimate, though increasing slowly with acquisition time, is robust to random selection of acquisition time if acquisition time is longer than transient time. Nevertheless, to enhance comparability among patients and centers, a standardized acquisition time must be used for all patients and centers.

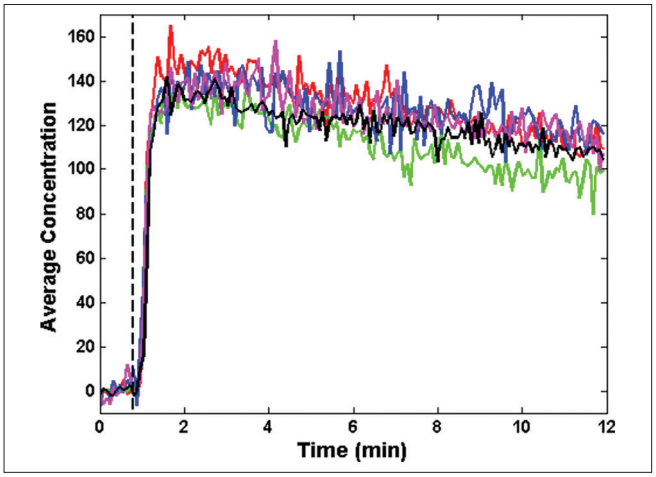

Figure 9: Concentration spatially averaged over all tissues except the kidney versus time, each shown by a color curve for one of the five rabbits. The vertical dashed line indicates the time of tracer emergence at 0.8 min (image 10)

Performance comparison with semiquantitative parameters

By using the rabbit data, the six semiquantitative parameters MTIR, washout gradient, upslope gradient, IAUC, maximum signal intensity, and onset time are evaluated for neovascularization assessment of atherosclerotic plaques and compared with performance of DIEEF plaques. The reader is referred to the references indicated in the introduction section for the technical details of these parameters. The correlation between each of the six semiquantitative parameters and neovessel count of aorta plaques of the five rabbits with corresponding P value was calculated. The MTIR of each rabbit was obtained by the maximum average plaque concentration $y(k)$ divided by the time reaching the maximum, and the correlation coefficient with the neovessel count is $r = 0.50$ with $P = 0.39$. The washout gradient a was estimated by the least square (LS) between $y(k)$ and a line $ak + b$ for time $k = 8$, 8.08, 8.16,…, 12 min and then $r = -0.30$ with $P = 0.63$. The upslope gradient a was estimated by the LS between $y(k)$ and a line $ak + b$ for time $k = 0.88$, 0.96, 1.04, 1.12, 1.2 min and then $r = 0.72$ with $P = 0.17$. The IAUC was obtained by summation of $y(k)$ for $k = 0.16$, 0.24,…, 2.16 min and then $r = 0.91$ with $P = 0.029$. The maximum signal intensity was obtained by taking the maximum $y(k)$ for all k and then $r = 0.83$ with

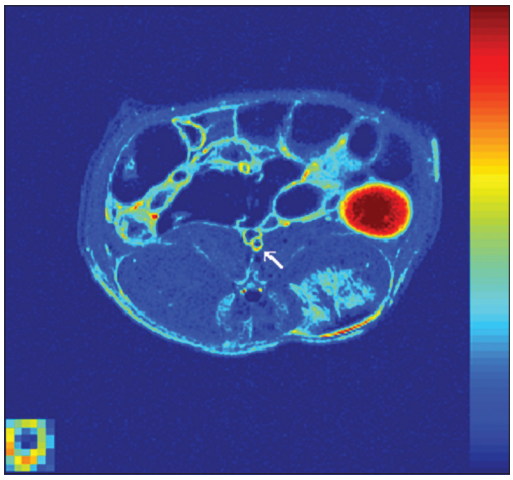

Figure 10: The DIEEF image of the representative rabbit. The arrow indicates the aorta with its magnified image at the bottom-left corner

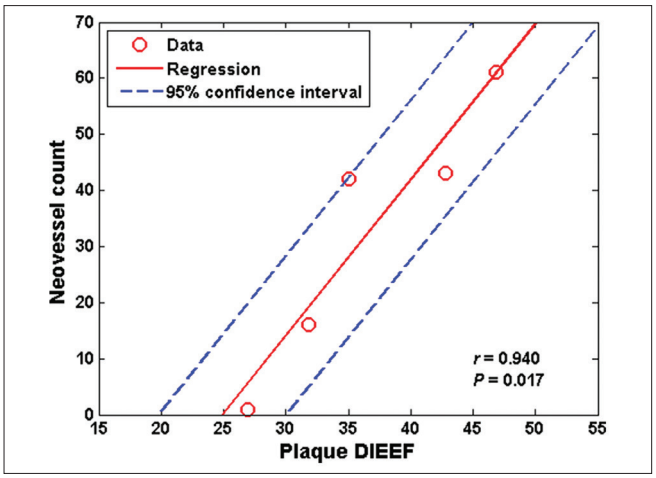

Figure 11: The DIEEF of aorta plaques versus neovessel count, linear regression, and 95% confidence interval

$P = 0.082$. The onset time was obtained by measuring the time interval from 0.4 min to the time when $y(k)$ just reaches 5, and then $r = -0.89$ with $P = 0.043$. Thus, the upslope gradient, maximum intensity, onset time, and IAUC have high r and low P value and are good indicators for plaque neovascularization whereas the MTIR and washout gradient have low r and high P value. With $r = 0.940$ and $P = 0.017$, DIEEF outperforms the six semiquantitative parameters in neovascularization assessment of atherosclerotic plaques in this test.

Table 3 compares characteristics of DIEEF, quantitative parameters and semiquantitative parameters. The quantitative parameters have the advantages of clear physiological relation, high reproducibility with low dependencies on scanner, patient, and center and the disadvantages of difficulty in model fitting, strong assumption, high computational complexity, and susceptibility to noise; whereas semiquantitative parameters have the advantages of modeling free, weak assumption, low computational complexity and the disadvantages of unclear physiological relation and low reproducibility.[1] In contrast, DIEEF possesses the advantages of both quantitative and semiquantitative parameters.

DISCUSSION

A DIEEF image depends only on physiological parameters – bidirectional permeabilities of capillary, IEEF of tissues in the region of view, and has a clear physiological meaning. Consequently, like a quantitative parameter, DIEEF is reproducible. For the same reason, the dose of tracer injection is unlikely to affect considerably performance of DIEEF in neovascularization assessment except that decrease of dose will decrease SNR. In practice, a tissue of interest shall be a small portion (e.g. a segment of arterial wall) in the region of view that is relatively large and stable to make the DIEEF of tissue of interest more reliable and reproducible.

Table 2: Performance versus total acquisition time T and effective acquisition time T'

T (min)	T' (min)	r	P
1.04	0.24	0.571	0.315
1.20	0.40	0.849	0.069
1.36	0.56	0.884	0.046
1.52	0.72	0.908	0.033
2.00	1.20	0.933	0.021
2.96	2.16	0.944	0.016
4.00	3.20	0.945	0.015
4.96	4.16	0.947	0.015
6.00	5.20	0.947	0.014
6.96	6.16	0.942	0.017
8.00	7.20	0.941	0.017

Table 3: Comparison of DIEEF, quantitative and semiquantitative parameters

Charateristics	Quantitative	Semiquantitative	DIEEF
Physiological relation	Clear	Unclear	Clear
Model fitting problem	Difficult	No	No
Assumption strength	High	Low	Low
Computational complexity	High	Low	Low
Reproducibility	High	Low	High
Estimation reliability	Low	High/low	High

DIEEF – Distribution of intravascular and extravascular extracellular volume fractions

The proposed method of DIEEF estimation does not require knowledge of AIF but assumes that all tissues in the region of view have the same average AIF. This assumption is satisfied when capillaries of tissues in the region of view are branches of a main artery. When data are incomplete, that is, acquisition ends before tracer is completely washed out through the kidney, a residual error is incurred. However, as illustrated by the simulation and the test on the model of atherosclerotic rabbits, impact of incomplete data on accuracy and performance of DIEEF is significant only during the transient time in which performance of DIEEF improves quickly as acquisition time increases. Performance of DIEEF is eventually high and stable post the transient time. This is true for both the tracer infusion and bolus injections, and DIEEF slightly favors the bolus injection.

Estimation of a quantitative parameter usually needs to fit a DCE-MRI curve to a pharmacokinetic model at each time instant, which might result in an invalid solution. In contrast, DIEEF estimation needs only the average of DCE-MRI curve, and therefore like a semiquantitative parameter, DIEEF does not have the model-fitting problem.

The averaging nature in DIEEF estimation also brings DIEEF several other advantages. Average of N samples increases SNR by the maximum of $10\log_{10}(N)$ dB and therefore DIEEF can be reliably estimated in the presence of noise. Without incurring a significant decrease of DIEEF image quality the temporal resolution of DCE-MRI data can be large and in return the spatial resolution can be small. This suggests that DIEEF is

promising in viewing and analyzing fine details of arterial plaques, which is important in diagnosis and treatment of atherosclerosis disease at the early-stage as the dimension of arterial plaques is small. This is also important for early-stage diagnosis and prognosis of tumor when tumor size is small. For the same reason a small spatial resolution may be traded off with increasing concentration of tracer injection. For example, doubling concentration of tracer injection increases SNR by a factor of four. To retain the same SNR, temporal resolution can be increased by a factor of four and therefore spatial resolution can be decreased accordingly. The effect of large temporal resolution and the tradeoff between spatial resolution and concentration of tracer injection are worth of further analysis and examination in animal and patient experiments. The averaging nature also makes DIEEF computationally simple and feasible for real-time clinical utilization.

The animal experiment result demonstrates that performance of DIEEF is robust to a random selection of acquisition time post the transient time but in this case is slightly worse than a fixed acquisition time. To enhance objectiveness, reproducibility and comparability among patients and scanners, standardization of acquisition time, tracer injection and region of view on the basis of a number of experiments is necessary for a particular type of tissues or organ.

CONCLUSION

A DIEEF image characterizes the distribution of neovascularization, permeability asymmetry of capillaries, and extravascular extracellular volume fractions. DIEEF has a clear physiological meaning, can be easily and reliably estimated without knowing the artery input function, is applicable to various types of tissues, and is positively correlated to neovessel count in the animal experiment. Post the transient time, performance of DIEEF is high and stable in both tracer infusion and bolus injections. DIEEF might be useful as a biomarker for noninvasive neovascularization assessment by DCE-MRI.

REFERENCES

1. Collins DJ, Padhani AR. Dynamic magnetic resonance imaging of tumor perfusion. Approaches and biomedical challenges. IEEE Eng Med Biol Mag 2004;23:65-83.
2. Leach MO, Brindle KM, Evelhoch JL, Griffiths JR, Horsman MR, Jackson A, *et al.* The assessment of antiangiogenic and antivascular therapies in early-stage clinical trials using magnetic resonance imaging: Issues and recommendations. Br J Cancer 2005;92:1599-610.
3. Tofts PS, Kermode AG. Measurement of the blood-brain barrier permeability and leakage space using dynamic MR imaging. 1. Fundamental concepts. Magn Reson Med 1991;17:357-67.
4. Tofts PS. Modeling tracer kinetics in dynamic Gd-DTPA MR imaging. J Magn Reson Imaging 1997;7:91-101.
5. Tofts PS, Brix G, Buckley DL, Evelhoch JL, Henderson E, Knopp MV, *et al.* Estimating kinetic parameters from dynamic contrast-enhanced T (1)-weighted MRI of a diffusable tracer: Standardized quantities and symbols. J Magn Reson Imaging 1999;10:223-32.
6. Flickinger FW, Allison JD, Sherry RM, Wright JC. Differentiation of benign from malignant breast masses by time-intensity evaluation of contrast enhanced MRI. Magn Reson Imaging 1993;11:617-20.
7. Kuhl CK, Mielcareck P, Klaschik S, Leutner C, Wardelmann E, Gieseke J, *et al.* Dynamic breast MR imaging: Are signal intensity time course data useful for differential diagnosis of enhancing lesions? Radiology 1999;211:101-10.
8. Daniel BL, Yen YF, Glover GH, Ikeda DM, Birdwell RL, Sawyer-Glover AM, *et al.* Breast disease: Dynamic spiral MR imaging. Radiology 1998;209:499-509.
9. Evelhoch JL. Key factors in the acquisition of contrast kinetic data for oncology. J Magn Reson Imaging 1999;10:254-9.
10. Walker-Samuel S, Leach MO, Collins DJ. Evaluation of response to treatment using DCE-MRI: The relationship between initial area under the gadolinium curve (IAUGC) and quantitative pharmacokinetic analysis. Phys Med Biol 2006;51:3593-602.
11. Patlak CS, Blasberg RG, Fenstermacher JD. Graphical evaluation of blood-to-brain transfer constants from multiple-time uptake data. J Cereb Blood Flow Metab 1983;3:1-7.
12. Wang Y, Huang W, Panicek DM, Schwartz LH, Koutcher JA. Feasibility of using limited-population-based arterial input function for pharmacokinetic modeling of osteosarcoma dynamic contrast-enhanced MRI data. Magn Reson Med 2008;59:1183-9.
13. Shukla-Dave A, Lee N, Stambuk H, Wang Y, Huang W, Thaler HT, *et al.* Average arterial input function for quantitative dynamic contrast enhanced magnetic resonance imaging of neck nodal metastases. BMC Med Phys 2009;9:4.
14. Ashton E, Raunig D, Ng C, Kelcz F, McShane T, Evelhoch J. Scan-rescan variability in perfusion assessment of tumors in MRI using both model and data-derived arterial input functions. J Magn Reson Imaging 2008;28:791-6.
15. Yankeelov TE, Luci JJ, Lepage M, Li R, Debusk L, Lin PC, *et al.* Quantitative pharmacokinetic analysis of DCE-MRI data without an arterial input function: A reference region model. Magn Reson Imaging 2005;23:519-29.
16. Yang C, Karczmar GS, Medved M, Stadler WM. Estimating the arterial input function using two reference tissues in dynamic contrast-enhanced MRI studies: Fundamental concepts and simulations. Magn Reson Med 2004;52:1110-7.
17. Kovar DA, Lewis M, Karczmar GS. A new method for imaging perfusion and contrast extraction fraction: Input functions derived from reference tissues. J Magn Reson Imaging 1998;8:1126-34.
18. Yankeelov TE, DeBusk LM, Billheimer DD, Luci JJ, Lin PC, Price RR, *et al.* Repeatability of a reference region model for analysis of murine DCE-MRI data at 7T. J Magn Reson Imaging 2006;24:1140-7.
19. Yang C, Karczmar GS, Medved M, Stadler WM. Multiple reference tissue method for contrast agent arterial input function estimation. Magn Reson Med 2007;58:1266-75.
20. Yankeelov TE, Cron GO, Addison CL, Wallace JC, Wilkins RC, Pappas BA, *et al.* Comparison of a reference region model with direct measurement of an AIF in the analysis of DCE-MRI data. Magn Reson Med 2007;57:353-61.
21. Walker-Samuel S, Leach MO, Collins DJ. Reference tissue quantification of DCE-MRI data without a contrast agent calibration. Phys Med Biol 2007;52:589-601.
22. Walker-Samuel S, Parker CC, Leach MO, Collins DJ. Reproducibility of reference tissue quantification of dynamic contrast-enhanced data: Comparison with a fixed vascular input function. Phys Med Biol 2007;52:75-89.
23. Yankeelov TE, Luci JJ, DeBusk LM, Lin PC, Gore JC. Incorporating the effects of transcytolemmal water exchange in a reference region model for DCE-MRI analysis: Theory, simulations, and experimental results. Magn Reson Med 2008;59:326-35.
24. Faranesh AZ, Yankeelov TE. Incorporating a vascular term into a reference region model for the analysis of DCE-MRI data: A simulation

study. Phys Med Biol 2008;53:2617-31.
25. Planey CR, Welch EB, Xu L, Chakravarthy AB, Gatenby JC, Freehardt D, *et al.* Temporal sampling requirements for reference region modeling of DCE-MRI data in human breast cancer. J Magn Reson Imaging 2009;30:121-34.
26. Davies MJ, Richardson PD, Woolf N, Katz DR, Mann J. Risk of thrombosis in human atherosclerotic plaques: Role of extracellular lipid, macrophage, and smooth muscle cell content. Br Heart J 1993;69:377-81.
27. Moreno PR, Falk E, Palacios IF, Newell JB, Fuster V, Fallon JT. Macrophage infiltration in acute coronary syndromes. Implications for plaque rupture. Circulation 1994;90:775-8.
28. Kerwin W, Hooker A, Spilker M, Vicini P, Ferguson M, Hatsukami T, *et al.* Quantitative magnetic resonance imaging analysis of neovasculature volume in carotid atherosclerotic plaque. Circulation 2003;107:851-6.
29. Kerwin WS, O'Brien KD, Ferguson MS, Polissar N, Hatsukami TS, Yuan C. Inflammation in carotid atherosclerotic plaque: A dynamic contrast-enhanced MR imaging study. Radiology 2006;241:459-68.
30. Kerwin WS, Oikawa M, Yuan C, Jarvik GP, Hatsukami TS. MR imaging of adventitial vasa vasorum in carotid atherosclerosis. Magn Reson Med 2008;59:507-14.
31. Chen H, Cai J, Zhao X, Underhill H, Ota H, Oikawa M, *et al.* Localized measurement of atherosclerotic plaque inflammatory burden with dynamic contrast-enhanced MRI. Magn Reson Med 2010;64:567-73.
32. Calcagno C, Cornily JC, Hyafil F, Rudd JH, Briley-Saebo KC, Mani V, *et al*. Detection of neovessels in atherosclerotic plaques of rabbits using dynamic contrast enhanced MRI and 18F-FDG PET. Arterioscler Thromb Vasc Biol 2008;28:1311-7.
33. Sun Y. Estimation of physiological parameters in the subspace of arterial input function in dynamic contrast-enhanced magnetic resonance imaging. Proc. IEEE Signal Processing in Medicine and Biology Symposium, SPMB 2011, Brooklyn, NY, Dec. 10; 2011.
34. Sun Y, Ye Z. Distribution of intravascular and extravascular extracellular volume fractions for neovascularization assessment by dynamic contrast-enhanced magnetic resonance imaging. Proc. IEEE Signal Processing in Medicine and Biology Symposium, SPMB2012, New York, NY, Dec. 1; 2012.
35. Sourbron SP, Buckley DL. On the scope and interpretation of the Tofts models for DCE-MRI. Magn Reson Med 2011;66:735-45.
36. Koh TS, Bisdas S, Koh DM, Thng CH. Fundamentals of tracer kinetics for dynamic contrast-enhanced MRI. J Magn Reson Imaging 2011;34:1262-76.
37. Yang X, Knopp MV. Quantifying tumor vascular heterogeneity with dynamic contrast-enhanced magnetic resonance imaging: A review. J Biomed Biotechnol 2011;2011:732848.
38. Gudbjartsson H, Patz S. The Rician distribution of noisy MRI data. Magn Reson Med 1995;34:910-4.
39. Proakis JG. Digital Communications. 4th ed. New York: McGraw Hill; 2000.
40. Sourbron S. Compartmental modelling for magnetic resonance renography. Z Med Phys 2010;20:101-14.

How to cite this article: Sun Y. Distribution of Intravascular and Extravascular Extracellular Volume Fractions by Total Area under Curve for Neovascularization Assessment by Dynamic Contrast-Enhanced Magnetic Resonance Imaging. J Med Sign Sence 2014;4:159-70.

Source of Support: Support for this project was provided by a PSC-CUNY Award, jointly funded by The Professional Staff Congress and The City University of New York, **Conflict of Interest:** None declared

BIOGRAPHIES

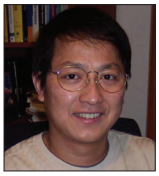

Dr. Yi Sun received the B.S. and M.S. degrees in electrical engineering from the Shanghai Jiao Tong University, Shanghai, China, in 1982 and 1985, respectively, and the Ph.D. degree in electrical engineering from the University of Minnesota, Minneapolis, MN, in 1997. From 1985 to 1993, Dr. Sun was a lecturer at the Shanghai Jiao Tong University, China. In the summer of 1993, he was a visiting scientist at the Concordia University, Montreal, Canada. He was a Postdoctoral Research Fellow at the University of Utah, Salt Lake City, UT from March to September 1997, and a Postdoctoral Research Associate at the University of Connecticut, Storrs, CT from October 1997 to August 1998. Since September 1998, Dr. Sun has been an Assistant Professor now with tenure in the Department of Electrical Engineering at the City College of City University of New York. Dr. Sun's research interests are in modeling, parameter detection and estimation, algorithm development, and performance analysis for various human-designed and biomedical systems. His research previously focused on image processing, wireless communications, and robotic searching, and now focuses on biomedical nanoscopy and quantitative bioimaging.

E-mail: ysun@ccny.cuny.edu